Journal of Molecular Catalysis A: Chemical 316 (2010) 75–82

Contents lists available at ScienceDirect

Journal of Molecular Catalysis A: Chemical

journal homepage: www.elsevier.com/locate/molcata

Structure and contribution to photocatalytic activity of the interfaces in nanofibers with mixed anatase and TiO_2(B) phases

Zhanfeng Zheng[a], Hongwei Liu[a], Jianping Ye[b], Jincai Zhao[b], Eric R. Waclawik[a], Huaiyong Zhu[a,*]

[a] Inorganic Materials Research Program, School of Physical and Chemical Sciences, Queensland University of Technology, GPO Box 2434, Brisbane, QLD 4001, Australia
[b] Institute of Chemistry, The Chinese Academy of Science, Beijing 100080, China

ARTICLE INFO

Article history:
Received 5 June 2009
Received in revised form 8 September 2009
Accepted 5 October 2009
Available online 12 October 2009

Keywords:
Interface structure
Anatase
TiO_2(B)
Photocatalytic activity
Nanofibers

ABSTRACT

Fibril photocatalyst of mixed TiO_2(B) and anatase phases, pure TiO_2(B) and pure anatase are obtained by calcining titanate nanofibers prepared via hydrothermal reaction at different temperatures between 300 and 700 °C. They are used to verify the theory that the difference between the conduction band edges of the two phases may produce charge transfer from one phase to the other, which results in effectively the photo-generated charge separation and thus facilitates the redox reaction involving these charges. Indeed, the mixed-phase nanofibers exhibit higher photocatalytic activity for degradation of sulforhodamine B (SRB) under UV light than the nanofibers of either pure phase alone, or the mechanical mixtures of the two pure phase nanofibers with a similar phase composition. The interfaces between the two phases have a function of preventing charge recombination and enhancing the activity for photocatalytic oxidation. These interfaces are not random contacts between the crystals of the two phases, but form from well-matched lattice planes of the two phases. For instance, (2 0 2) planes in anatase and (2 0 2) planes of TiO_2(B) are similar in d-spaces ~0.18 nm, and they join together to form a stable interface. Such an interface structure is advanced for charge transfer crossing the interfaces, which reduces the recombination between the photo-generated electrons and holes. The knowledge acquired in this study is important not only for design of efficient TiO_2 photocatalysts but also for understanding the photocatalysis process.

1. Introduction

TiO_2 is the most extensively studied material for photocatalysts because of its strong oxidizing power, low toxicity, and long-term photostability [1–3]. TiO_2 exists mainly in four polymorphs in nature, anatase (tetragonal, space group $I4_1/amd$), rutile (tetragonal, space group $P4_2/mnm$), brookite (orthorhombic, space group $Pbca$) and TiO_2(B) (monoclinic, space group $C2/m$) [4,5]. Generally, anatase phase is considered to have higher photoactivity than other phases [6,7]. However, TiO_2 powders consisting of mixed anatase and rutile nanocrystals have been found to exhibit a better photoactivity than pure anatase in many reaction systems. A well-known example is Degussa P25, which is fine TiO_2 powder with a mass ratio of anatase to rutile nanocrystals being 4:1 [8–10]. The enhanced activity of the catalysts with mixed anatase and rutile phases, relative to that of pure anatase, is of profound interest because it is important not only for design of efficient TiO_2 photocatalysts but also for understanding the photocatalysis process. This phenomenon has been extensively investigated [9–12] and it is believed that the difference between conduction band edges of the two phases may produce irreversible electron transfer from anatase to rutile (the band gap of anatase is 3.2–3.3 eV, slightly wider than that of rutile (3.0–3.1 eV), and the conduction band edge of anatase is about 0.2 eV higher than that of rutile) [13]. The relative alignment of the anatase and rutile conduction band edges suppresses the recombination of photo-generated electrons and holes. The efficient photo-generated charge separation facilitates the redox reaction involving these charges [8], although there are arguments as to whether the transfer is from anatase to rutile or in the reverse direction [10,11].

In principle, the efficient separation of charges via irreversible charge transfer should be applicable to other systems of mixed TiO_2 phases as long as there is a sufficient difference between the conduction band edges to cause irreversible charge transfer from one phase to another. If verified in other mixed TiO_2 phase systems, this mechanism could be an important principle for designing superior photocatalysts and for understanding photocatalysis processes. Besides the existence of numerous interfaces between two phases as a prerequisite for the irreversible transfer of the photo-generated charges across the interfaces, the interface structure should be crucial to the efficiency of the interfacial charge transfer process. However, few report on the structure of the interfaces in

* Corresponding author. Tel.: +61 07 31381581; fax: +61 07 31381804.
E-mail address: hy.zhu@qut.edu.au (H. Zhu).

1381-1169/$ – see front matter © 2009 Elsevier B.V. All rights reserved.
doi:10.1016/j.molcata.2009.10.002

mixed-phase photocatalysts exist in literature [10,11] because of the difficulty in determining the interface structures.

In the present study, we investigate the photoactivity of a series of nanofibers with mixed TiO_2(B) and anatase phases to verify the theory that the structure of mixed-phase titania polymorphs can enhance the photocatalytic activity. TiO_2(B) is a metastable monoclinic polymorph of titanium dioxide, which can be synthesized from titanate [14–18], sol–gel method [19] and is also found in nature [20]. Very recently, lithium storage by utilization of the channels in the TiO_2(B) structure has been reported [21,22]. However, TiO_2(B) exhibits only moderate photocatalytic activity, and there have been a few studies on the photocatalytic properties of this material [23,24]. The band gap of TiO_2(B) is in a range of 3–3.22 eV [23,25], slightly narrower than that of anatase (3.2–3.3 eV). TiO_2(B) can be converted into anatase by heating at high temperatures [26,27] so the synthesis of fibers of mixed anatase and TiO_2(B) is possible. Because the band gap of the TiO_2(B) phase is narrower than that of anatase [28], the difference between band edges of the two phases, is expected to induce charge transfer crossing at the interface between the two phases. Such interfacial charge transfer depends on the structure of the interfaces [10], intimate contact of one phase with the other is crucial to the transfer. However, determining the detailed structure of the interface between two TiO_2 polymorphs is a challenge. Fortunately, the nanofiber morphology is particularly suitable for transmission electron microscope (TEM) study on the interface structure formed in the phase transition region. Such a study reveals that in nanofibers TiO_2(B) and anatase phases intimately matched at the atomic level, forming the interfaces between the two phases. The well-matched structure could be a feature of the interfaces in other mixed-phase systems. Photocatalytic tests show that these interfaces are important for photoactivity of the nanofibers.

2. Experimental

2.1. Preparation of mixed-phase fibril photocatalyst

Hydrogen titanate nanofibers were synthesized through a hydrothermal reaction between concentrated NaOH and TiO_2 or an inorganic titanium compound and a post-synthesis ion exchange [29]. By heating the hydrogen titanate nanofibers at different temperatures, we obtained nanofibers with different mass ratios of anatase to TiO_2(B). Generally, 6 g of anatase particles (~325 mesh from Aldrich) was mixed with 80 ml of 10 M NaOH. The obtained suspensions were sonicated in an ultrasonic bath for 0.5 h and then transferred into an autoclave with a PTFE container inside. The autoclave was maintained at hydrothermal temperature of 180 °C for 48 h. The precipitate (sodium titanate nanofibers) was recovered, washed with distilled water (to remove excess NaOH), exchanged with H^+ (using a 0.1 M HCl solution) to produce hydrogen titanate nanofibers, and washed again with distilled water until pH ~ 7 was reached. The hydrogen titanate product was dried at 80 °C for 12 h and then calcined at a temperature from 300 to 700 °C for 4 h to prepare titania fibril photocatalysts of different phase composition.

2.2. Structure characterization

The transmission electron microscopy (TEM) study on the fibers was conducted using a Philips CM200 TEM with an accelerating voltage of 200 kV, and high-resolution TEM (HRTEM) investigation was carried out on a FEI Tecnai F20 operating at 200 kV. X-ray diffraction (XRD) patterns of the samples were recorded on a Philips PANalytical X'Pert PRO diffractometer using Cu Kα radiation (λ = 1.5418 Å) operating at 40 kV and 40 mA with a fixed slit. The Raman spectra of the samples were measured on a Spectra-Physics model 127, the excitation source was He–Ne laser (633 nm) and resolution was 2 cm^{-1}. To investigate the light absorption and emission behavior of the samples as well as their energy band gap, we measured the diffuse reflectance UV–vis (DR-UV–vis) spectra of the samples on a Varian Cary 5000 spectrometer. The nitrogen sorption isotherms were measured by volumetric method on an automatic adsorption instrument (Micromeritics, Tristar 3000) at liquid nitrogen temperature (77 K). Specific surface area was calculated by the Brunauer–Emmett–Teller (BET) method from the data in a P/P_0 range between 0.05 and 0.2. X-ray photoelectron spectroscopy (XPS) spectra were recorded on an ESCALAB 250 spectrometer and Al Kα radiation was used as the X-ray source. The C 1s peak at 284.5 eV was used as a reference for the calibration of the binding energy (BE) scale. FTIR emission spectra (IES) were carried out on a Digilab FTS-60A spectrometer equipped with a TGS detector, which was modified by replacing the IR source with an emission cell. The energy dispersive X-ray spectroscopy (EDS) experiment was carried out on a FEI Quanta 200 Environmental scanning electron microscopy (SEM). Electron paramagnetic resonance (EPR) spectra were recorded with a Bruker EPR ELEXSYS 500 spectrometer operating at a frequency of 9.5 GHz in the X-band mode. Measurements were performed with an ER 4131 VT variable temperature accessory at 135 K. The spectra were acquired when samples within the cavity were illuminated at 135 K by UV light, and an irradiation source (a Quanta-Ray Nd:YAG laser system with a wavelength of 355 nm) was used.

2.3. Photocatalytic activity measurement

The UV light source for photoactivity test was six tubular Hg lamps (NEC, FL20SBL) of 20 W, and the peak of the wavelength was at about 350 nm. The catalyst concentration was 0.5 g/L, and the initial concentration (C_0) of the sulforhodamine B (Aldrich) was 1.8×10^{-5} M. At regular irradiation time intervals, the dispersion was sampled, and the specimen was filtered through a Millipore filter (400 nm, Teflon) to remove the catalyst particles prior to the analysis. The filtrate was analyzed by UV–vis spectra (Varian Cary 100 spectrometer) for the absorbance intensity using reading at 565 nm. For the degradation of phenol, the initial concentration (C_0) of phenol was 25 ppm and the filtrates were analyzed by a high performance liquid chromatography (HPLC), Agilent, HPLC-Circa 2000, equipped with an Eclipse XDB-C8 column (5 μm, 4.6 mm × 150 mm). The eluent used was acetonitrile (HPLC grade) and 0.1% acetic acid (HPLC grade) solution.

3. Results

3.1. Phase transition, band gap, specific surface area and surface OH groups

X-ray diffraction (XRD) patterns (Fig. 1) of the samples calcined at temperatures from 300 to 700 °C and the precursor hydrogen titanate nanofibers illustrate the phase transitions from the titanate to TiO_2(B) and to anatase. Conversion of the hydrogen titanate phase to TiO_2(B) phase (JCPDS 74-1940) occurred at 300 °C and such observation is consistent with results reported in the literature [17]. Analysis of the Raman spectra (Fig. S3) of nanofibers calcined at 300 °C (T300) confirms that these samples were TiO_2(B) phase [21]. Diffractions from anatase phase (JCPDS 21-1272) can be seen for the sample calcined at 550 °C (T550) and the anatase fraction increased as the temperature was elevated from 550 to 700 °C. The product obtained after calcination at 700 °C (T700) was pure anatase. Mean crystallite size of TiO_2(B) and anatase

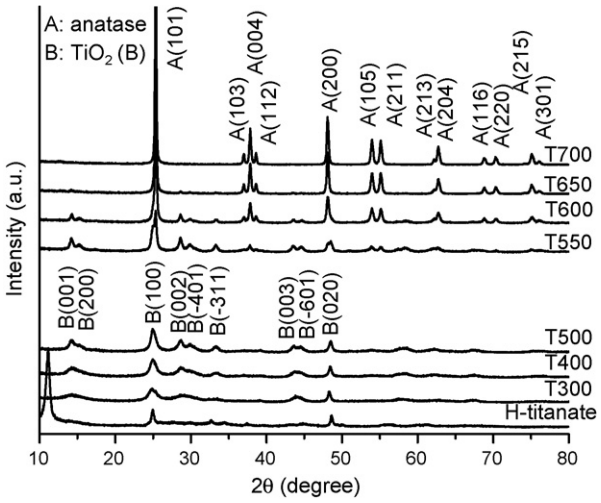

Fig. 1. XRD patterns of H-titanate calcined at different temperatures.

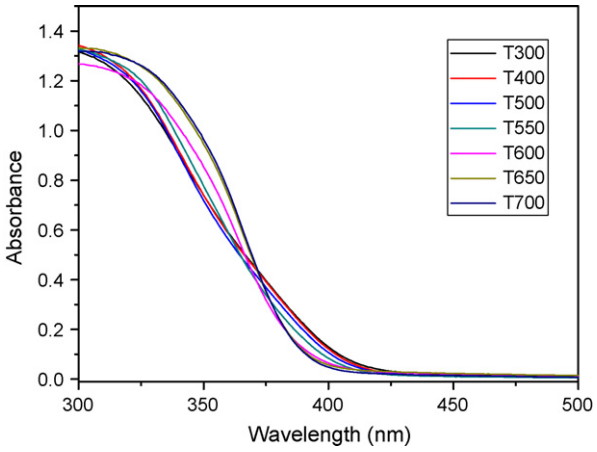

Fig. 2. UV–vis diffuse reflectance spectra of the TiO_2 nanofibers calcined at different temperatures from 300 to 700 °C.

phase were calculated from the line-broadening of XRD diffraction peaks at 24.9° and 25.3°, respectively and are listed in Table 1. The crystallite size increases gradually with increasing calcination temperature (Table 1). The phase fraction of TiO_2(B) and anatase in the mixed-phase samples were estimated from a calibration curve (See Supporting Information for details) and listed in Table 1. The change in phase composition was accompanied by changes in surface area and band gap. As anticipated, the BET specific surface areas of the samples, derived from nitrogen absorption data, decreased gradually with increasing calcination temperature (Table 1). From T300 to T700, the fibril TiO_2 lost about 40% of its surface area. Since the specific surface areas of the nanofibers are not large, the specific surface area seems not to be a determining factor on photocatalytic activity for the samples in the present study.

UV–vis diffuse reflectance (UV–vis DR) spectra of the samples are supplied in Fig. 2. The UV–vis absorption reflects the gap between the valence band and the conduction band of the titania. As anticipated, the phase transition illustrated above was accompanied by changes in the optical properties and thus the band gap of the samples. The light absorption by the samples gradually shifted to short wavelength direction (blue shift) as the calcination temperature was elevated (and anatase fraction increased). This is because the band gap of TiO_2(B) phase is narrower than that of anatase [28]. We calculated the absorption edge (listed in Table 1) by plotting $[F(R)E]^{1/2}$ against E, where $F(R)$ is the Kubelka–Munk function and E is the photon energy, and extrapolating the straight linear portion of the UV–vis spectra to $[F(R)E]^{1/2} = 0$ [30,31]. According to the results of this analysis, TiO_2(B) fibers (T500) possess a narrower band gap (about 3.05 eV), compared to the anatase nanofibers (3.19 eV). On the other hand, the light absorption of TiO_2(B) in the wavelength range between 300 and 370 nm was obviously lower than that of anatase. Because the UV irradiation was used for the photocatalytic reaction the weaker absorption may therefore lead to a lower reaction activity.

According to infrared emission spectra (IES) of H-titanate (Fig. S4), no surface OH group is left when the H-titanate is heated at a temperature above 500 °C. Although the surface OH groups can be reformed by dissociation of adsorbed water when the sample is exposed to moisture in air, yet the amount of these regenerated groups on the samples calcined at high temperature is much smaller, compared with that on the samples calcined at relative low temperature.

3.2. Morphology and interfaces of the mixed-phase catalysts (TEM analysis)

TEM images of the samples show that all the calcined samples inherited the fibril morphology of the parent hydrogen titanate nanofibers (Fig. 3). The nanofibers calcined at 300 °C, T300 (Fig. 3A–D), possessed smooth surfaces. According to the electron diffraction pattern (EDP, Fig. 3B) the fiber axis was [0 1 0] and each fiber was a TiO_2(B) single crystal (Fig. 3C and D). For the anatase nanofibers (T700, Fig. 3N–O), the nanofiber axis also aligned along the [0 1 0] direction, with (1 0 0) faces exposed. These fibers were anatase single crystals (according to the diffraction pattern, Fig. 3O) with rough surfaces (Fig. 3N) similar to a very recent report [32]. The XRD data indicated that during the heating above 550 °C, anatase phase formed from TiO_2(B) phase. Selected area electron diffraction (SAED) analysis further confirms that the nanofibers calcined at 600 °C, T600 (Fig. 3E–I), were composed of both anatase and TiO_2(B) phases in intimate contact with each other. Accordingly, numerous interfaces between these two phases existed in the nanofibers. For

Table 1
Physicochemical properties of as-synthesized TiO_2 fibril particles.

Sample	Temperature of heating (°C)	Phase composition[a]	Crystallite size (nm)[b]	S_{BET} (m^2/g)	E_g (eV)[c]
T300	300	B*	5.2 (B)	26.1	3.041
T400	400	B	7.4 (B)	25.1	3.046
T500	500	B	10.7 (B)	24.5	3.054
T550	550	B/A* (97.1:2.9)	–	23.4	3.091
T600	600	B/A (68.1:31.9)	56.8 (A)	20.1	3.183
T650	650	B/A (18.8:81.2)	77.3 (A)	17.5	3.185
T700	700	A	84.7 (A)	15.7	3.186

*B = TiO_2(B), A = anatase.

[a] Phase contents of the two phases were calculated from internal standard method obtained from Eqs. (1) and (2) which are shown in supporting information.

[b] Average crystallite size was estimated from XRD line-broadening of TiO_2(B) at 24.9° and anatase at 25.3° employing Scherrer equation.

[c] The band gap was estimated using UV–vis spectra data.

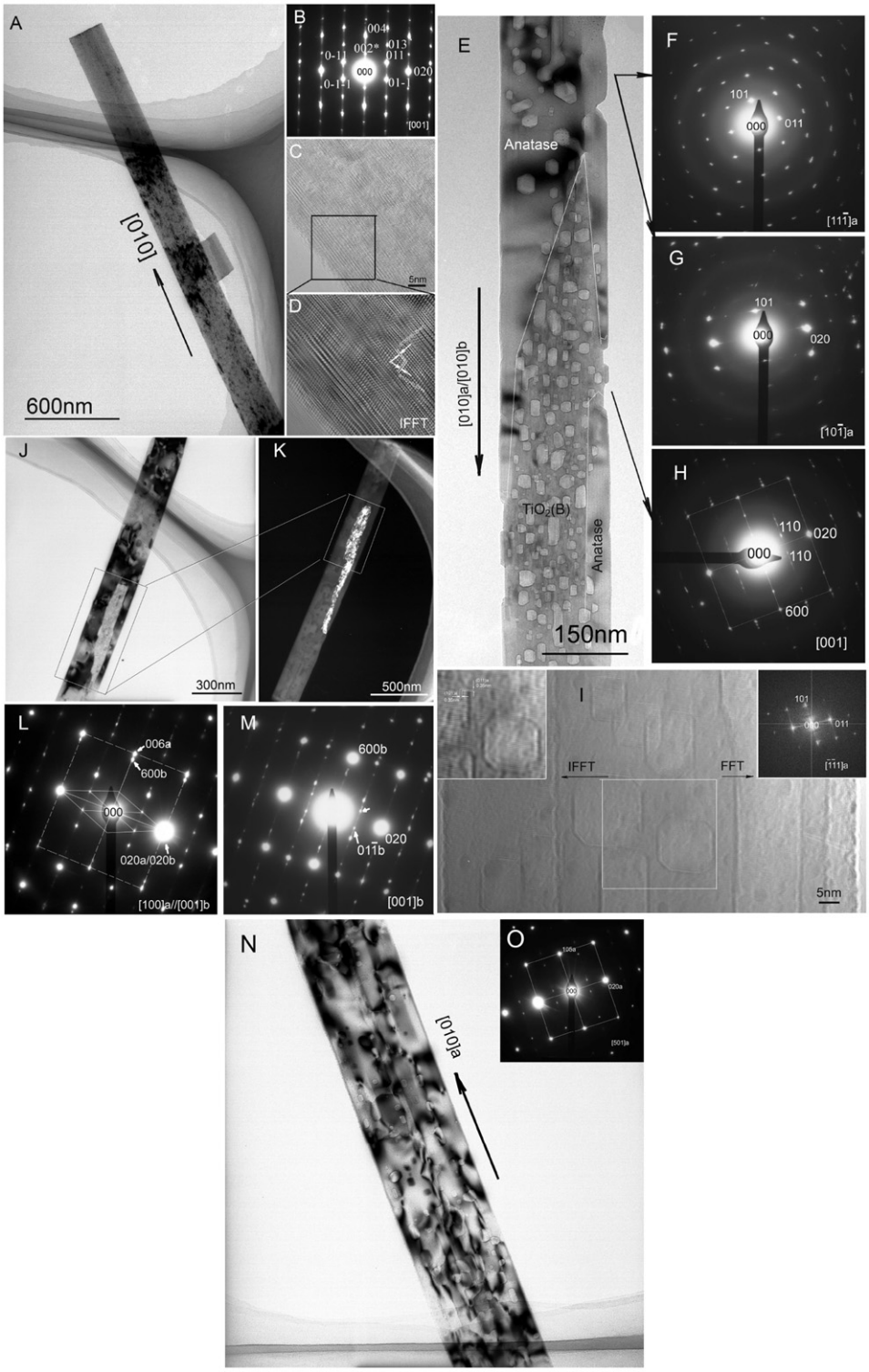

Fig. 3. Typical TEM, HRTEM images and EDP of fibril TiO_2: (A–D) T300, (E–I) T600, (J–M) T650, and (N–O) T700.

the T650 sample, calcined at a higher temperature, most of TiO_2(B) phase had been transformed to anatase, leaving only small residues of TiO_2(B) phase (the small area in the center of the fiber), as shown in bright field TEM image (Fig. 3J) and dark field TEM image (Fig. 3K). Here selected area electron diffraction (SAED) analysis (Fig. 3L and M) confirmed the co-existence of anatase and TiO_2(B) phases. The two phases join each other tightly; no voids between the crystals of the two phases were detected. Such a structure has better mechanical strength, compared to the fibril aggregates of anatase nanocrystals, which were obtained by a reaction of titanate with an acid solution in our previous study [33]. Although these fibril aggregates exhibited effective photocatalytic activity, they could be broken into fine particles by the mechanical stirring during use, due to the many voids between the anatase crystals. It is then difficult to separate the fine particles from the liquid after photocatalytic process. The fibers in the present study are therefore expected to

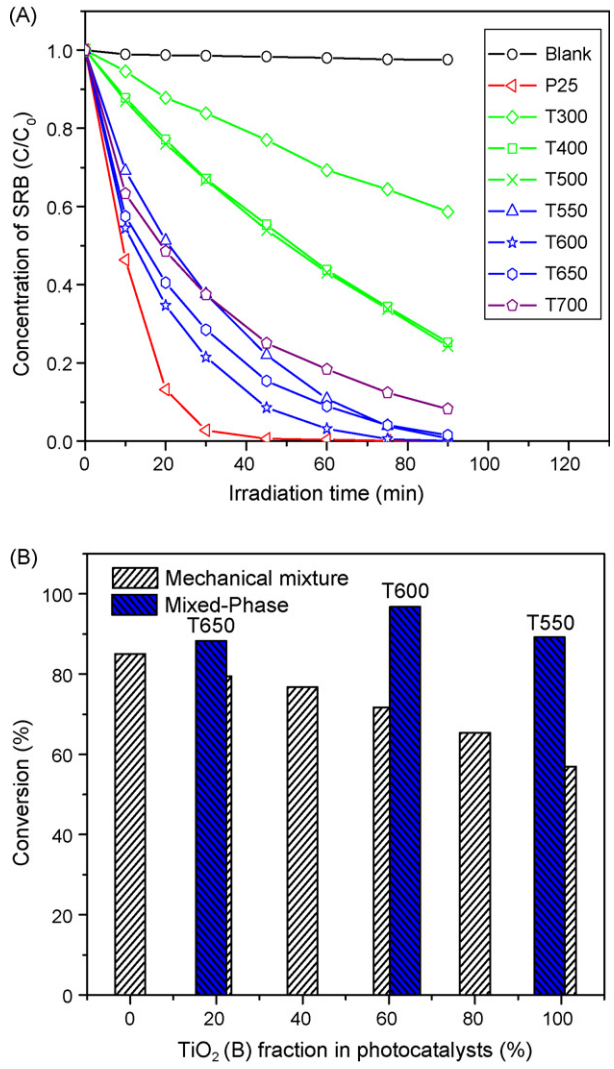

Fig. 4. (A) Photocatalytic decomposition of SRB with different fibril TiO_2 photocatalysts under UV irradiation and (B) comparison of conversion rate for the decomposition of SRB with mechanically mixed TiO_2 photocatalysts.

maintain the fibril morphology when they are in practical use. The nanofiber morphology has several other important advantages. The fibril shape has a large surface to volume ratio, relative to many other shapes such as sphere or cube. Because photocatalytic reactions take place on the surface of the catalysts [10,11], the reaction rate on the catalyst of larger surface area will be higher if other properties of the catalysts are the same. Moreover, the fibril photocatalysts can be readily separated from a fluid after reaction by simple filtration or sedimentation for reuse [34,35]. An additional merit of the nanofibers is that they are particularly suitable for TEM study on the phase transition and the interface structure because they are thin enough to show structural details in TEM images, and do not aggregate seriously to make it impossible to acquire the high quality TEM images and SAED patterns.

3.3. Photocatalytic performance

The photocatalytic performance of the TiO_2 nanofibers was compared to commercial Degussa P25 for decomposition of sulforhodamine B (SRB) dye under UV irradiation as illustrated in Fig. 4. The well-known Degussa P25 is composed of mixed anatase (80%) and rutile (20%) phases. Interestingly, the T600 nanofibers, composed of mixed anatase and TiO_2(B) phases, rather than the T700 nanofibers of pure anatase, exhibited the best photocatalytic activity among the TiO_2 fiber photocatalysts. More importantly, all three fiber samples with mixed phases, T550, T600 and T650 performed better than the pure anatase nanofibers, T700, and much better than the pure TiO_2(B) fiber samples T300, T400 and T500. The activity of the T600 is slightly lower than that of P25. The specific surface area of P25 is 51.0 m^2/g, which is 2–3 times of the surface areas of the TiO_2 nanofiber catalysts synthesized in the present study (for example, the specific surface area of T600 is 20.1 m^2/g). This is a possible reason for the higher activity of P25. In addition to the photocatalytic degradation of SRB under UV light illumination, the degradation of phenol under the same condition was also investigated (Fig. S5). There is no exception that all the mixed-phase nanofibers showed better activity than pure TiO_2(B) and anatase nanofibers.

All the mixed-phase fiber samples exhibited better photocatalytic activity than either pure anatase or pure TiO_2(B) fiber, this fact suggests that the superior activity may originate from the interfaces between the anatase and TiO_2(B) phases (which are identified by HRTEM analysis later). To ascertain the contribution of the interfaces between anatase and TiO_2(B) phases to the photocatalytic activity, we prepared mixtures with various mass ratios of TiO_2(B) to anatase by mechanically mixing of T500 [pure TiO_2(B) nanofibers] and T700 (pure anatase nanofibers). The nanofibers could be well-dispersed in an aqueous solution and exist in individual fibers as we observed when they were used to construct filtration membranes [36]. There should be no interfaces between anatase and TiO_2(B) phases in the suspensions of the mechanical mixtures for the test of photocatalytic performance. Therefore, the difference between the photocatalytic performances of the mixed-phase nanofibers and mechanically mixed nanofibers can be attributed to the interfaces in the former when the samples have the same phase composition. In Fig. 4B the photocatalytic activities of the mechanical mixtures for photocatalytic degradation of synthetic dye SRB are compared with those of the mixed-phase nanofibers. The percentage of the SRB decomposed after 60 min of UV light irradiation was used for comparing the activities of catalysts. As anticipated, the photocatalytic activity of the mechanical mixtures monotonically increased with increasing anatase fraction, because the activity of anatase nanofibers (T700) is much better than that of the TiO_2(B) (T500) as shown in Fig. 4A. In contrast, such a trend was not observed for the nanofibers with mixed phases. Moreover, the activity of the mixed-phase nanofibers was always significantly higher than that of the mechanical mixture with a similar phase composition (Fig. 4B). The specific surface area of the mixed-phase fibers shown in Fig. 4B was usually smaller than that of the mechanical mixture counterpart. The specific surface areas of the mechanical mixtures can be derived from the specific surface areas and the fractions of the two components in a mixture. It is 24.5 m^2/g for pure TiO_2(B) and 23.4 m^2/g for T550; 20.1 m^2/g for T600 and 21.0 m^2/g for the mixture containing 60% TiO_2(B) fibers. The surface area of T650 is and 17.5 m^2/g same as that of the mixture containing 20% TiO_2(B) fibers. Therefore, the better activity of the mixed-phase fibers, compared with that of the mechanical mixture counterpart, was not due to increase in specific surface area.

There are also other factors which may influence the photocatalysts' activity. Na^+ residual is a concern when ion exchange with HCl solution from titanate [37] as Na^+ impurities in TiO_2 act as recombination center, and thus reduce the photocatalytic activity [38]. In our experiment, no clear peak of Na KLL at BE = 507.71 eV (Na 1s cannot be used to identify the existence of Na element because Na 1s and Ti LMM are at the same region) was observed for the XPS survey scan (Fig. S6). It means that the Na content is very low and not detectable by the XPS. Na element was not

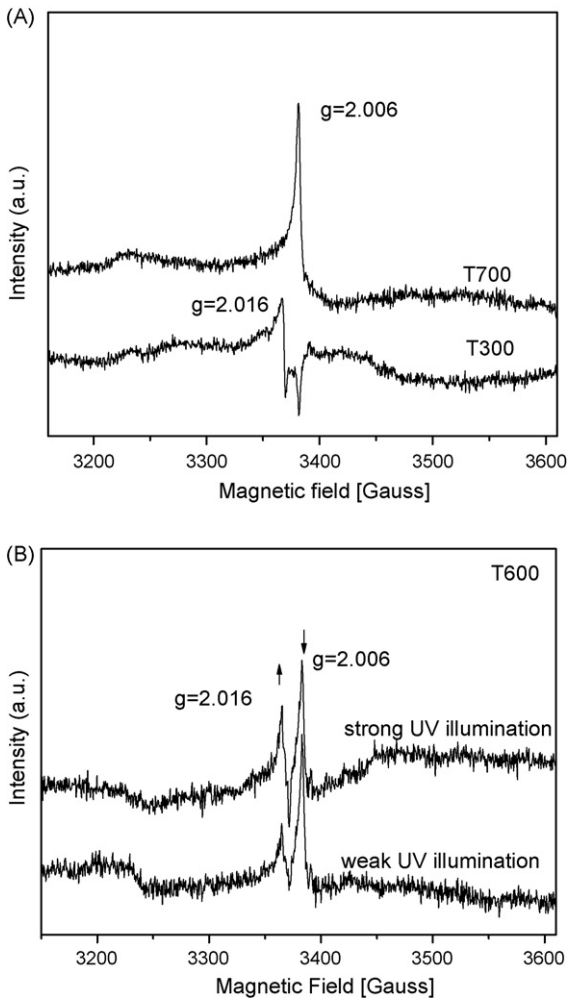

Fig. 5. EPR spectra of (A) pure TiO_2(B) (T300) and anatase (T700) nanofibers. (B) Mixed-phase nanofibers (T600) at weak and strong intensity of UV illumination. All samples were measured at 135 K after 20 min of UV exposure (355 nm, 100 W).

found by EDS analysis either (Fig. S7). The Na^+ content in all the catalysts prepared in this study is the same because they were obtained from the same H-titanate precursor simply by heating at different temperatures. Therefore, the influence from possible existence of trace Na^+ should be same and negligible for all the samples. According to Fujishima et al., calcination can result in loss of some surface OH groups which may affect the activity of the photocatalysts [39]. The samples heated at lower temperature possessed a higher OH group concentration, according to IES analysis as mentioned above, but exhibited poorer activity than that of the samples calcined at high temperature. Also P25, which exhibits the best activity for the decomposition of SRB in this study, has a relative low concentration OH group according to the IR vibration of OH groups in this solid. Therefore, in this study the OH concentration is not determining factor on the photocatalysts' activity. Consequently, it is deduced that the interface between the anatase and TiO_2(B) phases significantly enhances the photoactivity.

3.4. EPR measurement

Electron paramagnetic resonance (EPR) spectra of fibril catalysts T300, T600 and T700 are shown in Fig. 5. Under UV light illumination, a single peak at $g = 2.006$ and $g = 2.016$ was observed in the spectrum of T700 (anatase fibers) and T300 [TiO_2(B) fibers], respectively. These should attribute to their respective trapped holes (O^-), which is called single electron trapped oxygen vacancy [40]. For the mixed-phase nanofibers, T600, both peaks at $g = 2.006$ and $g = 2.016$ were observed after the sample was exposed to the UV irradiation for 20 min (Fig. 5B). When the intensity of UV irradiation was increased, the peak at $g = 2.016$ was enhanced, indicating an increase in holes concentration in TiO_2(B) occurred; while the intensity of the peak at $g = 2.006$ was reduced, indicating a decrease of holes (O^-) in the anatase phase. There are two pathways that can result in the intensity decrease of the peak at $g = 2.006$, which is the net result of the photo-generated charges in the mixed-phase structure. One is that holes (O^-) in the valence band of anatase phase transfer to the valence band of TiO_2(B), the other is that the electrons of TiO_2(B) migrate to the conduction band of anatase. But the excited electrons in TiO_2(B) obviously cannot migrate to anatase because of the CB edge of TiO_2(B) is lower than that of anatase. Therefore, it can be concluded that interfacial charge transfer processes increase population of holes (O^-) on TiO_2(B), and thus, increase the number of holes that reach the surface and available for oxidation. Given that the holes (O^-) have strong ability to oxidize organic pollutants (most likely through the formation of hydroxyl radicals), and the TiO_2(B) fraction in T600 nanofibers is much larger than the anatase fraction, the increase in hole concentration in TiO_2(B) phase under UV irradiation is likely to lead to high activity of the mixed-phase nanofibers for oxidizing dye molecules on their surfaces.

4. Discussion

4.1. Similarity to P25

The results of the photocatalytic activity test show that the TiO_2 nanofibers with mixed phases, which have interfaces between the TiO_2(B) and anatase phases, were superior photocatalysts compared to the fibers without interfaces, such as the pure TiO_2(B) and anatase nanofibers as well as the mechanical mixtures of TiO_2(B) and anatase nanofibers. It suggests that the interfaces between the crystals of the TiO_2(B) and anatase have the function of enhancing the photocatalytic activity. Given that the interfaces between two phases are not directly exposed to dye molecules, they should contribute to the photocatalytic activity by permitting irreversible transfer of photo-generated charges across the interfaces [10,11,41], similar to that of the interfaces between the anatase and rutile crystals in P25, rather than by merely providing sites for adsorption. The light absorption of TiO_2(B) is similar to that of rutile, both phases possess a band gap narrower than that of anatase, and are able to absorb the light of wavelength longer than 385 nm (Fig. 2). Therefore, the role of TiO_2(B) in the fibers is similar to that of rutile in P25. For P25, the photo-generated charge transfer across the interfaces between anatase and rutile phases originates from the difference between band edges of the two phases [10,41]. Such charge transfer across the interfaces is irreversible so that it results in effective separation of the photo-generated electrons and holes, reducing recombination and thus enhancing the photocatalytic activity. The results in the present study confirm that such a mechanism could also be applicable to other systems of mixed TiO_2 phases.

4.2. Interfacial electron transfer in the mixed-phase fibers (proposed mechanism)

The irreversible charger transfer across the interfaces can effectively separate the photo-generated electrons and holes, reduce

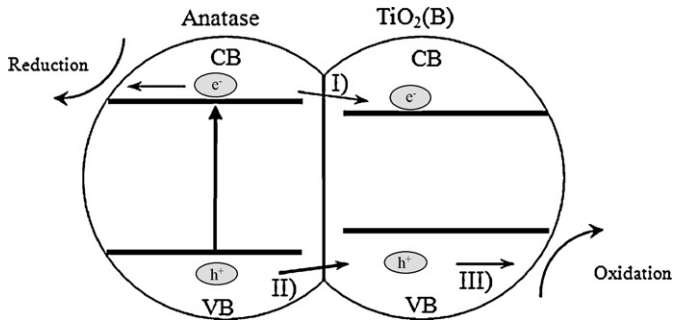

Fig. 6. Schematic description of the possible irreversible interfacial charge transfer process for the mixed-phase nanofibers under light illumination. Process (I) the interfacial electron transfer from the conduction band of anatase to TiO_2(B) phase (slow); Process (II) interfacial hole transfer from the valence band of anatase to TiO_2(B) phase (fast) and Process (III) holes move to the surface of TiO_2(B) phase to take part in the oxidation reaction.

their recombination and thus enhance the photocatalytic activity [10,41]. The possible interfacial charge transfer process in the mixed-phase structures is depicted in Fig. 6. This process is based on the EPR observation that the holes transfer from anatase to TiO_2(B). In fact, both the excited electrons and holes in anatase can be transferred to TiO_2(B). But due to the transfer speed of these two electrons are quite different in TiO_2, it seems like that only hole can be transferred. Because the effective mass of the electrons ($m_e^* > 10m_e$, m_e is free electron mass) is much larger than that of holes ($m_h^* = 0.8m_e$) in anatase TiO_2 [42]. The smaller effective mass of the holes in anatase is consistent with the high mobility and thus the time required for electrons to migrate to the same destinations in the same anatase crystals longer than those for holes [41,43]. Therefore, as shown in Fig. 6, the photo-generated holes can migrate more promptly to the adjacent TiO_2(B) phase than the photo-generated electrons. The overall outcome for the inter-phase charge transfer should be the holes move from anatase to TiO_2(B) and this has been detected by EPR. This transfer will reduce the recombination of photo-generated electrons and holes in anatase phase. In the following process, the holes in the valence band of TiO_2(B) can transfer to the surface, which enhances the oxidation activity of the fibers. It is rational and has been recognized by other researchers that the interface structure is crucial for the charge transfer and the photocatalytic activity of the mixed-phase TiO_2 photocatalysts.

4.3. Interface structure in the mixed-phase nanofibers

To better understand the roles of the interfaces and the photocatalytic process, efforts were made to extract a picture of the structure of these interfaces at an atomic level from the result of HRTEM images. Penn and Banfield have proposed an important mechanism for nanocrystalline coarsening and phase transition, the oriented attachment mechanism [44]: nanocrystals join at surfaces of crystallographic similarity to maximize the formation of chemical bonds between atoms of opposing surfaces, to achieve full coordination and reduce the interface energy. Such coherence between two nanocrystals of different phases results in reduction of Coulomb forces and minimization of dangling bonds to create stable interfaces. Bonding between two phases to reduce overall energy by minimizing surface energy associated with unsatisfied bonds is also apparent in this study. A HRTEM image on the region of an interface between TiO_2(B) and anatase in a fiber of T600 is illustrated in Fig. 7A. However, its resolution is not good enough to provide atomic arrangement of the interface. We therefore conducted a fast Fourier transformation (FFT) over the square area marked in Fig. 7A to obtain electron diffraction patterns of both anatase and TiO_2(B) from this area. After filtering out noise, which may come from defects and dislocation of atoms, sharp patterns were obtained and converted back to an image by inversing FFT (IFFT). The processed image (Fig. 7B) shows unambiguous structure of the interface at an atomic level by joining (2 0 2) plane in anatase with (2 0 2) plane in TiO_2(B). The plane (2 0 2) has a half of the d-spacing of the plane (1 0 1). For anatase, the d-spacing of plane (2 0 2) is 0.176 nm. For TiO_2(B), this value is 0.178 nm. The difference between them is 0.002 nm, far smaller than the layer distance of the matching plane. So it indicates that the two planes (2 0 2) of anatase and (2 0 2) of TiO_2(B) can join at the atomic level with the smallest mismatching. This well-matched structure thereby minimizes large crystallographic discrepancies, numbers of dangling bonds and voids in interface region. Hence, this is the advanced structure for efficient charge transfer crossing the interfaces as proved by EPR. The results also reveal that the mixed-phase particles were not aggregates of randomly oriented crystals of the two TiO_2 polymorphs, as usually thought. For aggregates of randomly oriented crystals of two phases there are infinite possible interfaces between the two phases, while there should be limited types of the interfaces formed by well-matched two phases (the matched interfaces). Because the matched interfaces should be the most stable interface structure, they should also exist in other TiO_2 photocatalysts of mixed anatase and TiO_2(B) phase. This deduction is of significant importance.

The difficulty in experimental determination of the interface structure was greatly reduced because of the fibril morphology and the size of the nanofibers. This is extremely difficult when the mixed-phase particles have irregular or round shapes and aggregate to each other. With the above deduction one can use the information of the matched interface structures to explain the properties of other TiO_2 photocatalysts with mixed TiO_2(B) and anatase phases.

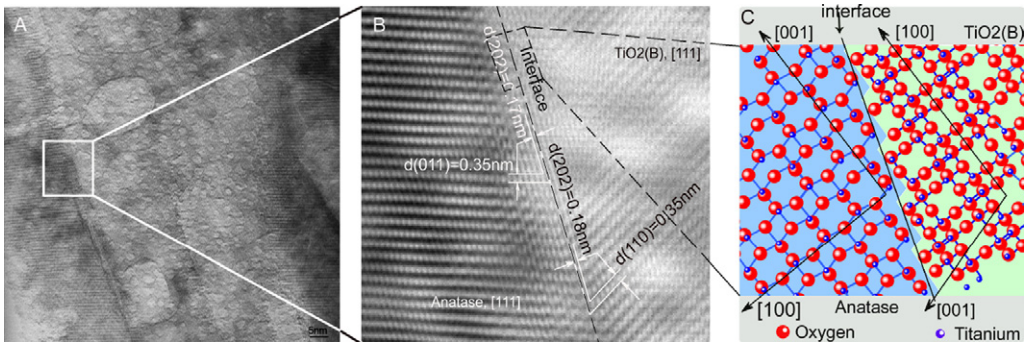

Fig. 7. HRTEM image and the atomic arrangement of an interface between TiO_2(B) and anatase phases in the T600 nanofibers.

5. Conclusions

In summary, this study addresses two important general issues regarding mixed-phase photocatalysts. First, it demonstrates the theory that the difference between band edges of two phases in intimate contact can facilitate charge transfer from one phase to another, and thus reduce the recombination of photo-generated electrons and holes. This is applicable to the photocatalysts of mixed TiO_2(B) and anatase phases. The interfaces between the two phases have a function of lowering charge recombination and enhancing the activity for photocatalytic oxidation of SRB. Second, the atomic arrangement of the interfaces between the two phases was determined for the first time. We found that the two phases closely match each other at the interface at an atomic level, and this structure facilitates the charge transfer. This could be general feature for stable interfaces between two phases in mixed-phase catalysts. Thus the above information is useful for understanding the mechanism of the photocatalytic reactions on the mixed-phase catalysts. The determination of interface structure of metal oxides is an important frontier in solid-state inorganic chemistry. The progress in this aspect is of general significance and may be extended to other metal oxide systems. In addition, a series of mixed-phase nanofibers were prepared by relatively simple process, and they are efficient photocatalysts in terms of activity, mechanical strength and separation after uses.

Acknowledgement

Supports from the Australian Research Council (ARC) are gratefully acknowledged.

Appendix A. Supplementary data

Supplementary data associated with this article can be found, in the online version, at doi:10.1016/j.molcata.2009.10.002.

References

[1] A.L. Linsebigler, G.Q. Lu, J.T. Yates, Chem. Rev. 95 (1995) 735–758.
[2] M.R. Hoffmann, S.T. Martin, W.Y. Choi, D.W. Bahnemann, Chem. Rev. 95 (1995) 69–96.
[3] M.A. Fox, M.T. Dulay, Chem. Rev. 93 (1993) 341–357.
[4] S. Bakardjieva, V. Stengl, L. Szatmary, J. Subrt, J. Lukac, N. Murafa, D. Niznansky, K. Cizek, J. Jirkovsky, N. Petrova, J. Mater. Chem. 16 (2006) 1709–1716.
[5] R.L. Penn, J.F. Banfield, Am. Miner. 84 (1999) 871–876.
[6] K. Tanaka, M.F.V. Capule, T. Hisanaga, Chem. Phys. Lett. 187 (1991) 73–76.
[7] K. Yanagisawa, J. Ovenstone, J. Phys. Chem. B 103 (1999) 7781–7787.
[8] R.I. Bickley, T. Gonzalez-Carreno, J.S. Lees, L. Palmisano, R.J.D. Tilley, J. Solid State Chem. 92 (1991) 178–190.
[9] T. Berger, M. Sterrer, O. Diwald, E. Knozinger, D. Panayotov, T.L. Thompson, J.T. Yates, J. Phys. Chem. B 109 (2005) 6061–6068.
[10] D.C. Hurum, A.G. Agrios, K.A. Gray, T. Rajh, M.C. Thurnauer, J. Phys. Chem. B 107 (2003) 4545–4549.
[11] D.C. Hurum, A.G. Agrios, S.E. Crist, K.A. Gray, T. Rajh, M.C. Thurnauer, J. Electron Spectrosc. Relat. Phenom. 150 (2006) 155–163.
[12] D.C. Hurum, K.A. Gray, T. Rajh, M.C. Thurnauer, J. Phys. Chem. B 108 (2004) 16483–16487.
[13] T. Kawahara, Y. Konishi, H. Tada, N. Tohge, J. Nishii, S. Ito, Angew. Chem. Int. Ed. 114 (2002) 2935–2937.
[14] R. Marchand, L. Brohan, M. Tournoux, Mater. Res. Bull. 15 (1980) 1129–1133.
[15] M. Tournoux, R. Marchand, L. Brohan, Prog. Solid State Chem. 17 (1986) 33–52.
[16] L.R. Wallenberg, M. Sanati, A. Andersson, J. Catal. 126 (1990) 246–260.
[17] T.P. Feist, P.K. Davies, J. Solid State Chem. 101 (1992) 275–295.
[18] D.V. Bavykin, J.M. Friedrich, F.C. Walsh, Adv. Mater. 18 (2006) 2807–2824.
[19] T. Kogure, T. Umezawa, Y. Kotani, A. Matsuda, M. Tatsumisago, T. Minami, J. Am. Ceram. Soc. 82 (1999) 3248–3250.
[20] J.F. Banfield, D.R. Veblen, D.J. Smith, Am. Miner. 76 (1991) 343–353.
[21] A.R. Armstrong, G. Armstrong, J. Canales, P.G. Bruce, Angew. Chem. Int. Ed. 43 (2004) 2286–2288.
[22] M. Zukalova, M. Kalbac, L. Kavan, I. Exnar, M. Graetzel, Chem. Mater. 17 (2005) 1248–1255.
[23] S. Yin, J.H. Wu, M. Aki, T. Sato, Int. J. Inorg. Mater. 2 (2000) 325–331.
[24] S. Yin, Y. Fujishiro, J.H. Wu, M. Aki, T. Sato, J. Mater. Process. Technol. 137 (2003) 45–48.
[25] G. Betz, H. Tributsch, R. Marchand, J. Appl. Electrochem. 14 (1984) 315–322.
[26] J.F. Zhu, J.L. Zhang, F. Chen, M. Anpo, Mater. Lett. 59 (2005) 3378–3381.
[27] H.L. Kuo, C.Y. Kuo, C.H. Liu, J.H. Chao, C.H. Lin, Catal. Lett. 113 (2007) 7–12.
[28] L. Kavan, M. Kalbac, M. Zukalova, I. Exnar, V. Lorenzen, R. Nesper, M. Graetzel, Chem. Mater. 16 (2004) 477–485.
[29] Y. Lan, X.P. Gao, H.Y. Zhu, Z.F. Zheng, T.Y. Yan, F. Wu, S.P. Ringer, D.Y. Song, Adv. Funct. Mater. 15 (2005) 1310–1318.
[30] F.P. Koffyberg, K. Dwight, A. Wold, Solid State Commun. 30 (1979) 433–437.
[31] Y.I. Kim, S.J. Atherton, E.S. Brigham, T.E. Mallouk, J. Phys. Chem. B 97 (1993) 11802–11810.
[32] W.Q. Han, L.J. Wu, R.F. Klie, Y.M. Zhu, Adv. Mater. 19 (2007) 2525–2529.
[33] H.Y. Zhu, X.P. Gao, Y. Lan, D.Y. Song, Y.X. Xi, J.C. Zhao, J. Am. Chem. Soc. 126 (2004) 8380–8381.
[34] H.Y. Zhu, Y. Lan, X.P. Gao, S.P. Ringer, Z.F. Zheng, D.Y. Song, J.C. Zhao, J. Am. Chem. Soc. 127 (2005) 6730–6736.
[35] Y.B. Mao, S.S. Wong, J. Am. Chem. Soc. 128 (2006) 8217–8226.
[36] X.B. Ke, H.Y. Zhu, X.P. Gao, J.W. Liu, Z.F. Zheng, Adv. Mater. 19 (2007) 785–790.
[37] E. Morgado, M.A.S. de Abreu, O.R.C. Pravia, B.A. Marinkovic, P.M. Jardim, F.C. Rizzo, A.S. Araujo, Solid State Sci. 8 (2006) 888–900.
[38] H. Tada, M. Tanaka, Langmuir 13 (1997) 360–364.
[39] A. Fujishima, K. Hashimoto, T. Watanabe, TiO_2 Photocatalysis: Fundamentals and Applications, BKC, Tokyo, 1999.
[40] S.L. Zhang, W. Li, Z.S. Jin, J.J. Yang, J.W. Zhang, Z.L. Du, Z.J. Zhang, J. Solid State Chem. 177 (2004) 1365–1371.
[41] B. Sun, A.V. Vorontsov, P.G. Smirniotis, Langmuir 19 (2003) 3151–3156.
[42] B. Enright, D. Fitzmaurice, J. Phys. Chem. 100 (1996) 1027–1035.
[43] H. Tang, K. Prasad, R. Sanjines, P.E. Schmid, F. Levy, J. Appl. Phys. 75 (1994) 2042–2047.
[44] J.F. Banfield, S.A. Welch, H.Z. Zhang, T.T. Ebert, R.L. Penn, Science 289 (2000) 751–754.